Atomization and Sprays, vol. 16, pp. 843–855, 2006

TWO-DIMENSIONAL DROPLET SIZE AND VOLUME FRACTION DISTRIBUTIONS FROM THE NEAR-INJECTOR REGION OF HIGH-PRESSURE DIESEL SPRAYS

*Jennifer Labs and Terry Parker**
Division of Engineering, Colorado School of Mines, Golden, CO 80401

Original Manuscript Submitted: 1/3/05; Final Draft Received: 7/19/05

Droplet diameter and volume fraction measurements are reported as a function of radial and axial position near the injector orifice within a high-pressure spray typical of diesel systems. Injection system parameters were peak pressures of ~ 80 MPa and a single orifice injector with a 0.16 mm diameter and an L/D ratio of ~ 4. Two cases are presented and discussed in detail; injection into room ambient conditions and injection with combustion (initial conditions: 873 K, 12.5 atm). Scattered light at two infrared wavelengths was collected from a spatially resolved probe volume and, through scattering theory, both Sauter mean diameter and liquid volume fraction were produced. Spray properties were determined as a function of time at a number of points, and these points form a grid based on multiple axial and radial positions within the spray. Results from multiple, yet identical, events were used to construct two-dimensional contour plots of the Sauter mean diameter and volume fraction within the spray.

INTRODUCTION

Fuel sprays are critical to diesel engine operation; a high-pressure jet formed by a small orifice is used to produce the air-fuel mixture required for combustion. The region near the injector tip is where liquid breakup, evaporation, ignition, and burning occur. Unfortunately, this region has not been extensively investigated due to the extreme difficulty of making measurements in this area. These measurements are difficult to make because of the high number densities of droplets and the transient nature of the spray event. This article provides Sauter mean diameter (SMD) and liquid volume fraction data from the spray interior and is part of an ongoing effort to characterize the liquid portion of diesel sprays. This effort began with line-integrated measurements of the spray [1] and has progressed to spatially resolved or "point" measurements within the spray [2]. Results presented here are the first of their kind in that two-dimensional contour plots of droplet diameter and volume fraction are presented based on infrared scattering and extinction measurements.

It is important to note that this work is an extension of work that was presented in Labs and Parker [2]; however, the nozzle orifice used for results presented here was smaller than the previously used orifice. Conclusions were drawn in [2] that will be revisited and supported by the data presented here (i.e., radial and temporal dependencies). Experimentally, minor changes were made to the optics to ensure that the system was in focus. Further steps forward since the previous article [2] include the reporting of data in two dimensions (axial and radial positions) as well as the addition of combusting and evaporating spray data.

Motivation and Background

The diesel engine is a classical thermodynamic cycle that has been in use for many decades; its overriding desirable characteristic is an in-practice higher efficiency than that for spark ignition engines (due primarily to the higher compression ratios and reduced throttling losses [3]). Thus, the diesel is appealing to society in terms of both economy and global-warming-based emissions. Unfortunately, pollutant emissions from diesels are hard to control since the fuel is injected into the high-temperature and high-pressure charge near top dead center in the piston stroke. Thus, mixture formation is a

*Corresponding author; e-mail: tparker@mines.edu

Copyright © 2006 by Begell House, Inc.

transient event with the added complication of a variable ignition delay (which depends on the in-cylinder environment and fuel properties as well as fuel-air mixing). Emission behavior for the diesel engine is characterized by the "soot-NO_x trade-off" [3]; a decrease in one of these pollutants is typically accompanied by an increase in the other. Improving the performance of diesel engines requires a detailed understanding of diesel combustion and the spray-driven fuel-air mixing that is linked to overall engine performance.

Diesel sprays near the injector tip are typical of an optically "thick" system (note that a standard definition of *optically thick* does not exist; as used in this work the term describes regions where attenuation impedes classical measurement methods). Regions where the attenuation of visible light as it passes through the spray is high (typically, 85% or more) are typical of sprays, and it is this optical thickness that impedes spray measurements. However, a group at Argonne National Laboratory [4, 5] have employed x-rays to examine the liquid fuel structure in the region very near the injector orifice under room ambient conditions; note that this work has shown that the injection velocities associated with high-pressure injection can generate shock waves as the spray propagates into the high-temperature and -pressure gas. This work uses an x-ray-absorbing additive to monitor the mass of fuel along a line-of sight; in contrast, the work described by this article produces spatially resolved (i.e., information at a volume in space) sauter mean diameters and liquid volume fractions without any fuel additives.

Measurement techniques described in this article utilize infrared wavelengths, which, like the use of x-rays, is a substantial departure from the more commonly used visible probe wavelengths. A change to infrared probes, provided the droplets or particles are sufficiently small, can significantly lower the optical thickness of the system, therefore allowing measurements to be made in the near injector region [1, 6].

Hardware Description

Experiments were conducted in a diesel engine simulator facility that consisted of an injection system and a combustion vessel. Experiments utilized a repeatable, single-shot, high-pressure, metering fuel injection system, which closely follows the design produced by Oren et al. [7]. A pressure amplifier was used to drive a custom-drilled Lucas CAV nozzle with a single orifice of 0.16 mm diameter and an L/D of ~ 4. Peak injection pressures of ~ 80 MPa were obtained with this system for this set of experiments. All experiments were conducted using dodecane in a custom-manufactured combustion vessel. For the combusting and evaporating experiments, the vessel was operated at 12.5 atm and 873 K (see [8] for a more detailed description of the simulator facility).

Optical measurements were based on dual wavelength coaxial beam scattering and extinction, and optical access was provided normal to the injector axis in two orthogonal directions through barium fluoride windows (chosen for their visible and infrared transmittance properties). Figure 1 depicts a schematic of the measurement layout. This system used a tunable CO_2 laser operated at 9.27 μm and an Nd:Yag laser operated at the fundamental frequency (1.06 μm), both continuous wave (cw), to produce the probe volumes. The beams were focused and combined to produce coaxial beams with experimentally verified identical waists and positions at the center of the spray (within the combustion vessel). By using sufficiently fast detectors (on the order of 100 kHz), light that traversed the spray zone (extinction measurement) and scattered light from within the probe volume at both wavelengths was measured.

Extinction measurements rely on Beer's law [9] to relate the absorption/scattering of light as it passes through a medium to the number density, optical cross section, and path length. Utilizing the ratio of Beer's law for two wavelengths, the extinction response of fuel droplets may be used, in the absence of other absorption features, to determine the size of the droplets in the system. Refer to Labs and Parker [2], for further detail.

Spatial resolution and an increased dynamic range for the sizing of droplet diameters are provided by the scattering measurements (compared to extinction measurements), and scattering measurements allow calculation of number density and volume fraction. As with the extinction measurements, the scattering measurements utilize infrared wavelengths that are attenuated less than visible wavelengths by the spray. Since a scattering signal is proportional to number density and optical cross section, a ratio of signals at different wavelengths and angles can be used to produce size information for the droplets in the probe volume. Note that the traditional scattering equations have been modified to include an optical thickness correction; details are provided in Labs and Parker [2].

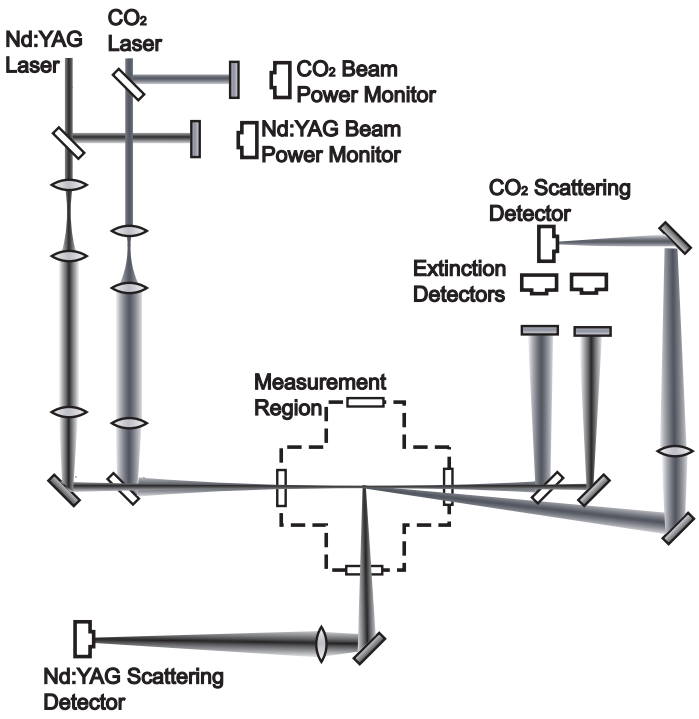

Fig. 1 Optical layout for extinction and scattering measurements.

Data reduction for the scattering signals is based on a comparison of multiple signals. Thus, data reduction necessarily implies homogeneity over the spatial region occupied by the probe volumes for each of the signals that, in effect, sets a minimum scale for the measurement. For these measurements, the region of assumed homogeneity is the probe volume diameter (0.15 mm diameter) and the maximum probe volume length along the laser beam waists (~ 0.43 mm; note that this length is shorter than that observed in our previous work and was achieved by repositioning the lens that forms an image of the HgCdTe detector at the probe volume). Factors such as size distribution width, droplet sphericity, and beam steering on the data set have been addressed, in detail, in Parker et al. [6] and have been found to be negligible for the present system.

As a companion to the work described in this article, multiple scattering has been experimentally investigated. At issue is the degree to which, as a function of spray conditions and position within the spray, multiply scattered photons are erroneously included in the reported scattering signals. For room ambient conditions, results indicate that multiple scattering effects are notable for the area of the spray radially within 1 mm of the centerline to an axial distance of 25 mm. For the combusting case, multiple scattering effects were reported to be negligible throughout the region of interest. Refer to Labs and Parker [10], for complete details and results.

RESULTS

Experiments were conducted and data was collected for a range of background conditions at the same injection condition. Peak injection pressure for all experimental results presented here was just above 80 MPa; the injection event lasted for ~ 3 ms (see Fig. 2). Background conditions of interest can be categorized as cold (or room ambient), evaporating, and combusting. The "cold" condition was simply injection into room ambient temperature and pressure (298 K and 0.8 atm). The evaporating and combusting cases used a background temperature of 873 K and an absolute pressure of 12.5 atm. For the

evaporating case, the fuel was injected into an oxygen-free environment; the vessel was filled with nitrogen. For combusting experiments, the fuel was injected into air.

Along the central axis of the spray, beginning at 15 mm from the injector orifice, data were collected every 5 mm axially to a distance of 45 mm. At each axial location, data was collected radially at 0.3 mm intervals beginning at the centerline and extending to the spray edge (where the scattering signal was effectively zero). Note that the centerline was "found" optically. First, the maximum extinction locations were found by translating the system in a direction perpendicular to the laser beams. A point of maximum scattering at the spray periphery was then found by translating the experiment parallel to the beams. These two x and y coordinates define the spray centerline.

For each point at a given axial and radial position, signals were collected every 2 μs for a 40 ms period surrounding the injection event so that all transient processes within the spray were observed. Periods before the start of injection were used to quantify zero and full-scale signals (both beams were chopped) with no spray present, as well as system noise for each detector. All the data presented here have been processed and averaged in time over a 100 μs interval.

Figure 2 depicts a typical injection pressure trace as well as a typical vessel pressure trace for a combusting experiment. Critical times are labeled on the plot, with injection beginning at time zero (start of injection, as verified by HeNe extinction measurements; note that this correlates with the small dip in the injection pressure curve). Ignition was determined from the very first pressure rise observed in the vessel pressure trace. It is clear from this plot that ignition occurs while injection is still occurring; therefore, from a semantic perspective, these events can be considered combusting and not simply evaporating. However, the majority of the heat release (large pressure rise) for this operating pressure occurs after the injection event ends. Thus, the combusting and evaporating events are not distinguishable from a spray perspective. Figure 3 compares SMD and volume fraction results of evaporating and combusting events as a function of time on the spray centerline 25 mm from the injector tip. Figure 4 compares the results as a function of axial position (along centerline) during the steady-state portion of the event. Because of the similarities between the cases and to simplify the discussion, the evaporating case will not be addressed directly; any discussion of the combusting case can be extended to the evaporating

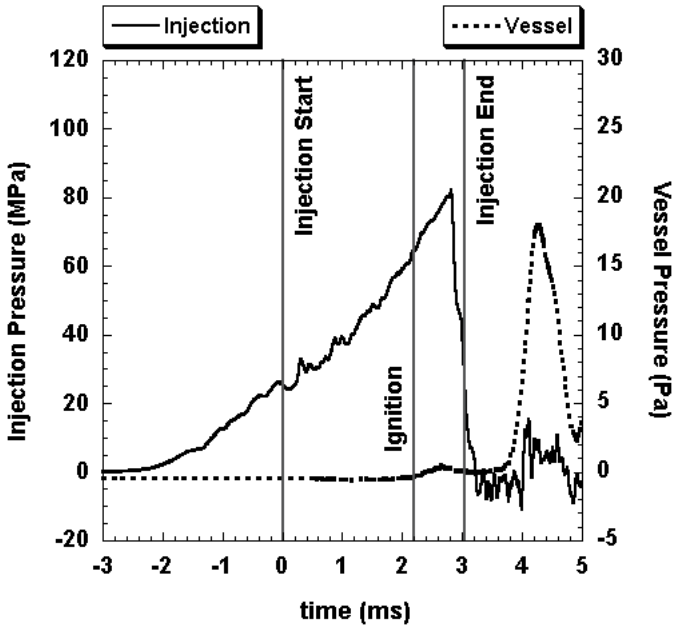

Fig. 2 Typical injection and vessel pressure traces as a function of time with start of injection, ignition, and end of injection labeled.

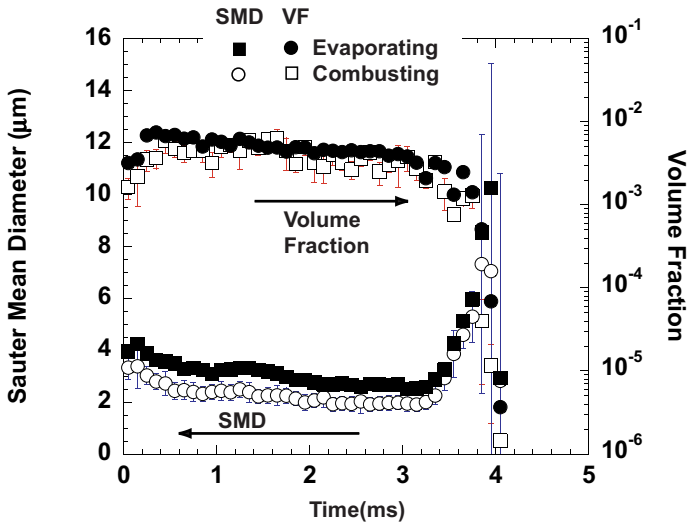

Fig. 3 Comparison of volume fraction and SMD for the combusting and evaporating cases as a function of time at 25 mm from the injector orifice along the centerline. Error bars are included for the combusting data and include the effect of calibration error, noise, and unsteadiness during the 100 μs averaging interval; error levels for the evaporating data are of a similar magnitude.

case. It is interesting to note that the combusting and evaporating cases are so similar. For this system, the major heat-release event occurs after the end of injection, which explains the insensitivity of the spray to combustion. Note also that the increase in droplet size at the end of the spray is typical of the spray

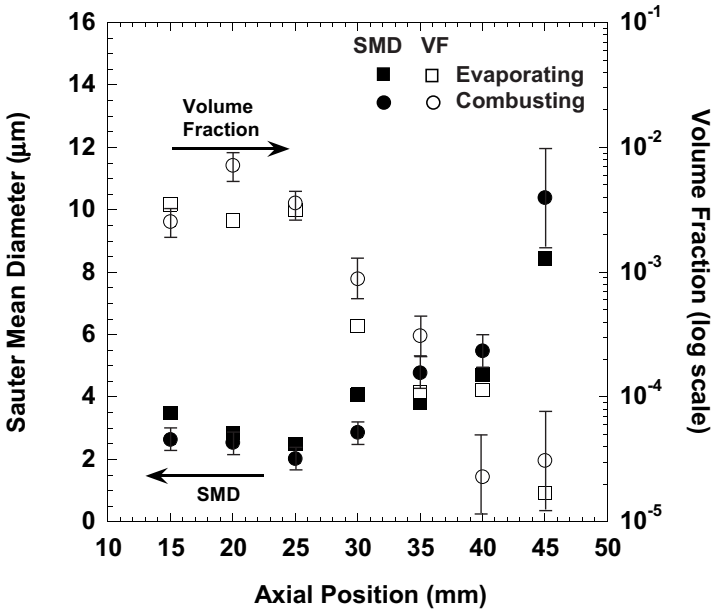

Fig. 4 Comparison of volume fraction and SMD for the combusting and evaporating cases as a function of axial position during the steady portion of the spray at the centerline. Values are the average for 2.5–2.6 ms, and error bars are included for the combusting data. Error levels for the evaporating data are of a similar magnitude.

shutoff period, where the injection pressure drops precipitously. Therefore, only the combusting and room ambient cases will be addressed in further detail.

Both the combusting and cold cases support the conclusion drawn from earlier work [2] that three distinct time periods are evident. Temporally, there is a spray-development period, a steady-state period, and a spray-dissipation period. Figure 5 shows volume fraction (solid symbols) and Sauter mean diameter (open symbols) as a function of time for both cases at the centerline 25 mm axially from the orifice. It is important to note that all positions in the spray (including those not shown here) exhibit the same temporal dependencies. The spray develops for the first 0.75 ms of the injection event. Volume fraction climbs to a steady value and measured diameter falls. The spray is then fully developed and continues at steady state until the injection event ends at ~ 3 ms. All cases demonstrate relatively constant values during the steady-state time period, with the cold case exhibiting a small amount of scatter. Finally, the spray ends during the dissipation period. During this period, the volume fraction drops off dramatically and measured droplet size increases, consistent with the loss of injection pressure associated with injection shutoff.

Examining the combusting and cold cases, similarities in trends are evident with differences in absolute values. Axial dependencies during steady state (at 2.05 ms after start of injection) for both cases are shown in Fig. 6 (note that data at 15 mm for the cold case is not included due to expected high error levels from multiple scattering). The combusting case exhibits smaller droplets near the orifice; however, for axial positions of ~ 35–45 mm, the droplet sizes are very similar to the cold-case results. Volume fraction data indicates that the combusting spray contains significantly less liquid mass at the centerline than the cold spray at distances greater than 25 mm. Thus, as expected due to evaporation effects, the combusting spray does not penetrate as far as the room ambient spray. The data support the conclusion that more fuel remains in the liquid phase during the cold-spray event compared to the combusting event; for locations 25 mm or more from the tip, the difference in liquid volume fraction is one decade or more. Note as well the growth in SMD between 25 and 45 mm for the combusting case.

Figure 7 illustrates the trend of droplet growth with radial distance from centerline for both the combusting and cold cases at a distance of 25 mm from the injector orifice (during steady state at 2.05 ms after start of injection). Throughout the radial profile of the spray, the cold spray consistently produced

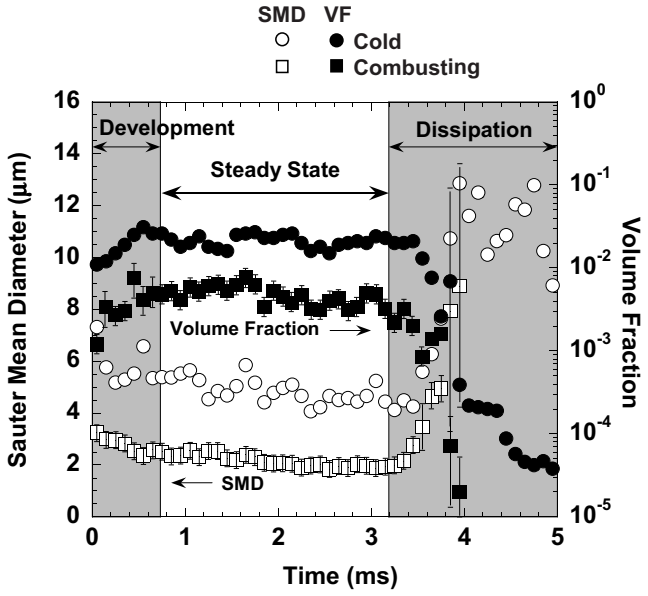

Fig. 5 Comparison of volume fraction and SMD for the combusting and cold cases as a function of time at 25 mm from the injector orifice along the centerline. Additionally, the three characteristic time periods are labeled. Error bars are included for the combusting data, and error levels for the evaporating data are of a similar magnitude.

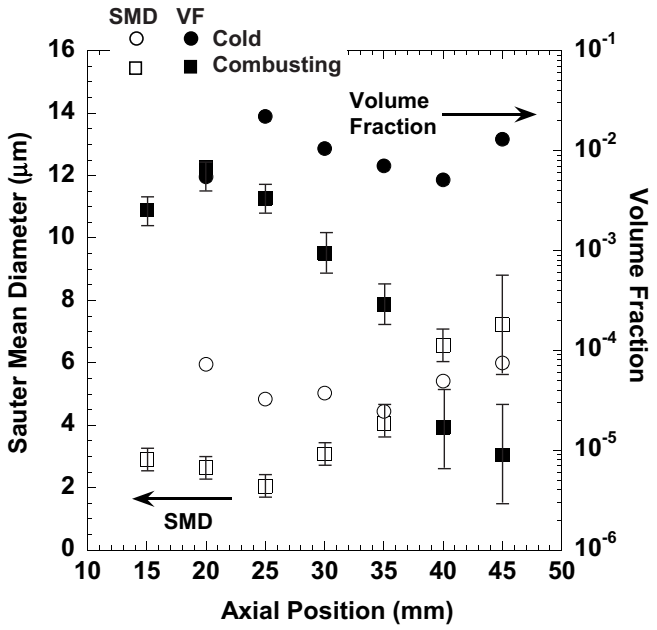

Fig. 6 Comparison of volume fraction and SMD for the combusting and cold cases as a function of axial position during the steady portion of the spray at the centerline. Values are the average for the time period 2.0–2.1 ms, and error levels for combusting data are shown. Error levels for the cold data are of a similar magnitude.

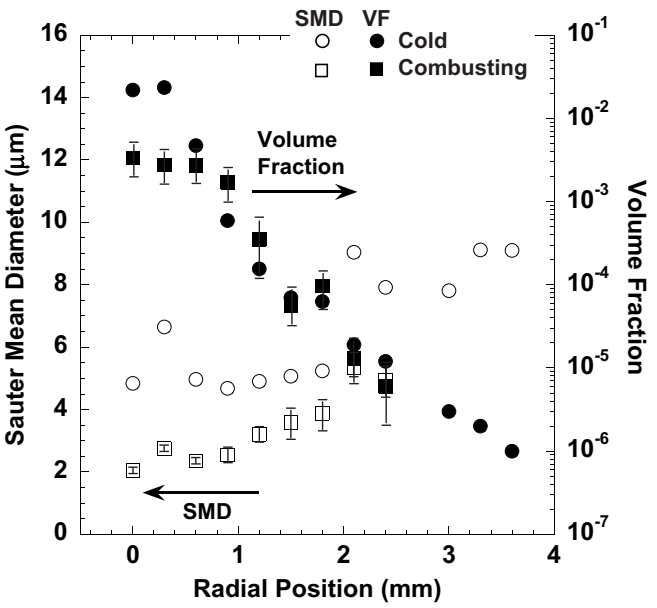

Fig. 7 Comparison of volume fraction and SMD for the combusting and cold cases as a function of radial position during the steady portion of the spray at 25 mm from the injector orifice. Values are the average for the time period 2.0–2.1 ms, and error levels for combusting data are shown. Error levels for the cold data are of a similar magnitude.

larger droplets than the evaporating case. The volume fraction trend for both cases is also shown in Fig. 7; as expected, the volume fraction falls with radial distance from centerline. Note that the volume fraction value changes by over three decades for both sprays over this 3.6 mm radial distance. At a distance of 25 mm from the injector orifice, the volume fractions at radial distances between 0.6 and 2.4 mm are remarkably similar; however, between 0 and 0.6 mm, the cold case is much thicker. Droplets were nonexistent at a radial distance of > 2.4 mm for the combusting case, but still existed out to a radial distance of 3.6 mm for the cold case. Clearly, the cold spray is thicker near the center of the jet and, overall, wider than the combusting spray. Once again, the data indicate that, as expected, comparatively more fuel is in the liquid phase for the cold spray event.

Figure 8 shows SMD and volume fraction data for 3.75 ms after the start of injection (0.7 ms after injection shutoff) for both the cold and combusting case. As in Fig. 7, these data provide a radial profile of diameter (SMD) and volume fraction at a distance 25 mm from the injector outlet. Comparison of these two figures shows the differences in the spray between the steady and dissipation periods. Volume fraction data from the dissipation period clearly follows a different radial trend (Fig. 8) compared to the steady-state injection period data (Fig. 7, note that the figures use the same scales to facilitate comparison). During steady state for both the cold and combusting case, the volume fraction decays steeply from its centerline value to its value on the spray edge. This change of over four decades in volume fraction occurs over a ~ 3 mm radial distance. For this case, the majority of the liquid mass is contained within a radius of < 1 mm. However, as shown in Fig. 8, for the dissipation period that occurs after injection shutoff the volume fraction versus radius curve "flattens." The majority of the liquid mass is contained in a 1.8 mm radial region with a roll-off in liquid volume fraction of ~ 2 decades between 1.8 and 2.5 mm. Overall, during the dissipation period after injection shutoff, the high-speed jet dissipates quickly causing the centerline volume fraction to fall. The far edges of the spray dissipate (radial regions > 2.4 mm) and the region between 1.2 and 1.8 mm gains mass, presumably from either the central region or upstream noncenterline regions.

Results from multiple, yet identical, events have been used to construct two-dimensional contour plots of the Sauter mean diameter and volume fraction within the spray. These plots are based on data obtained throughout the data acquisition grid, which was previously described; appropriate sorting allows

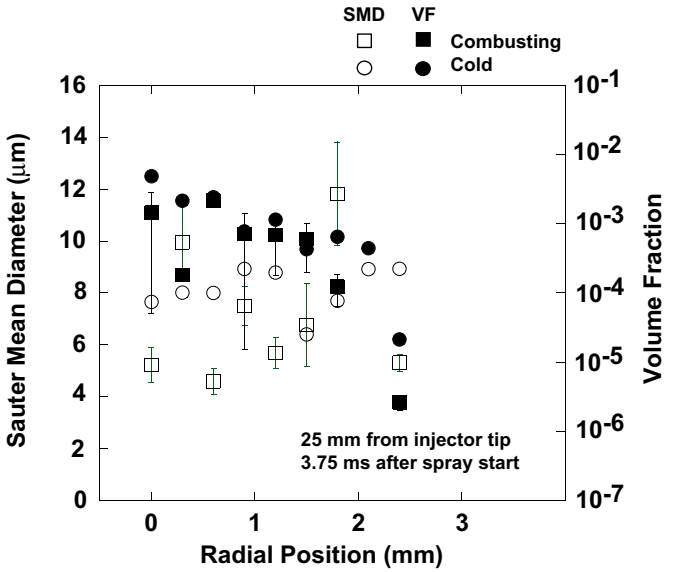

Fig. 8 Comparison of volume fraction and SMD for the combusting and cold cases as a function of radial position during the spray dissipation period at 25 mm from the injector orifice. Values are the average for the time period 3.7–3.8 ms, and error levels for combusting data are shown. Error levels for the cold data are of a similar magnitude.

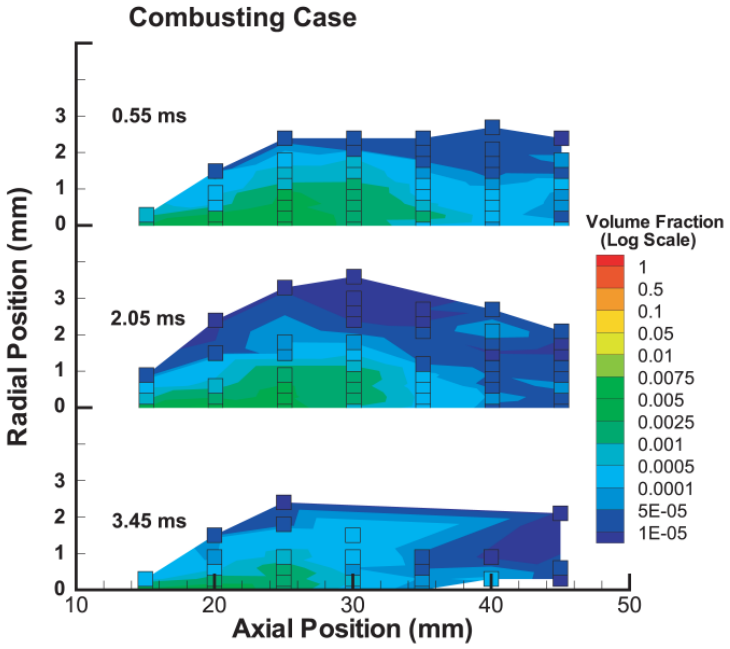

Fig. 9 Liquid volume fraction as a function of axial and radial position during each of the characteristic time periods [spray development (0.55 ms), steady state (2.05 ms), and spray dissipation (3.45 ms)] for the combusting spray.

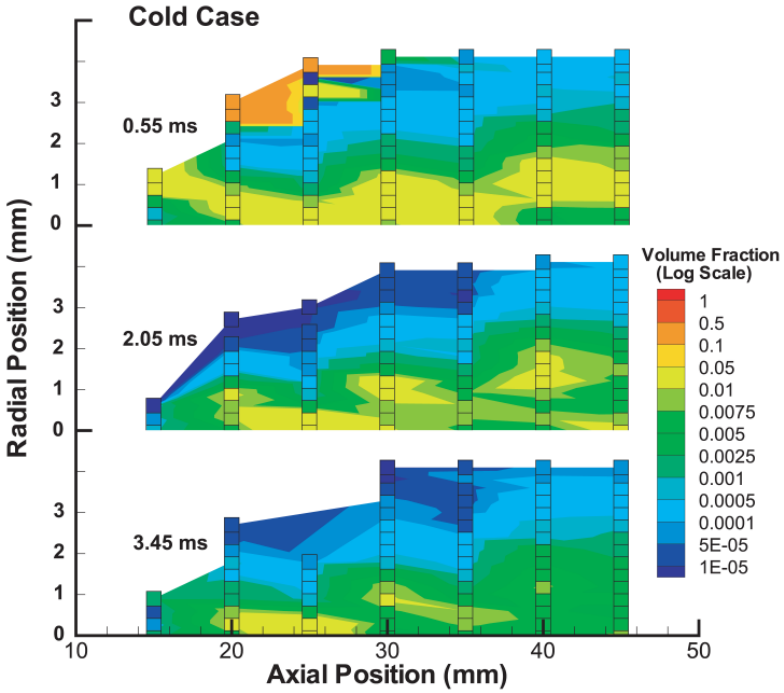

Fig. 10 Liquid volume fraction as a function of axial and radial position during each of the characteristic time periods [spray development (0.55 ms), steady state (2.05 ms), and spray dissipation (3.45 ms)] for the cold spray.

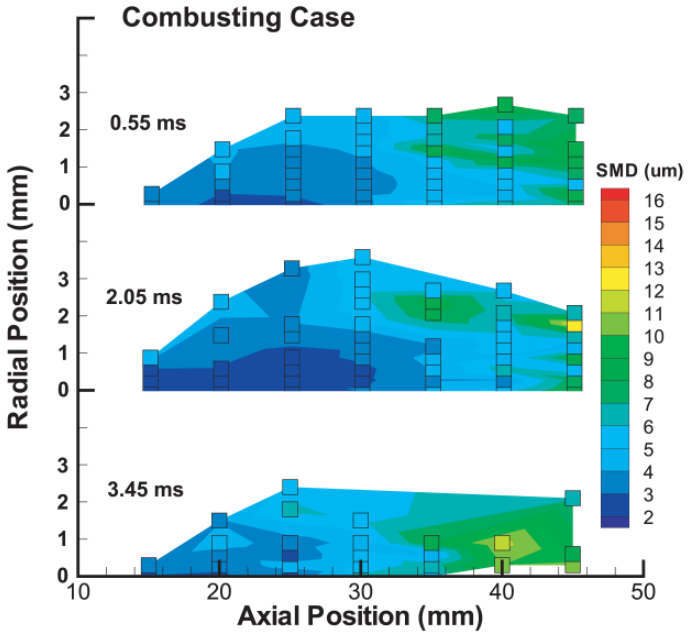

Fig. 11 Sauter mean diameter as a function of axial and radial position during each of the characteristic time periods [spray development (0.55 ms), steady state (2.05 ms), and spray dissipation (3.45 ms)] for the combusting spray.

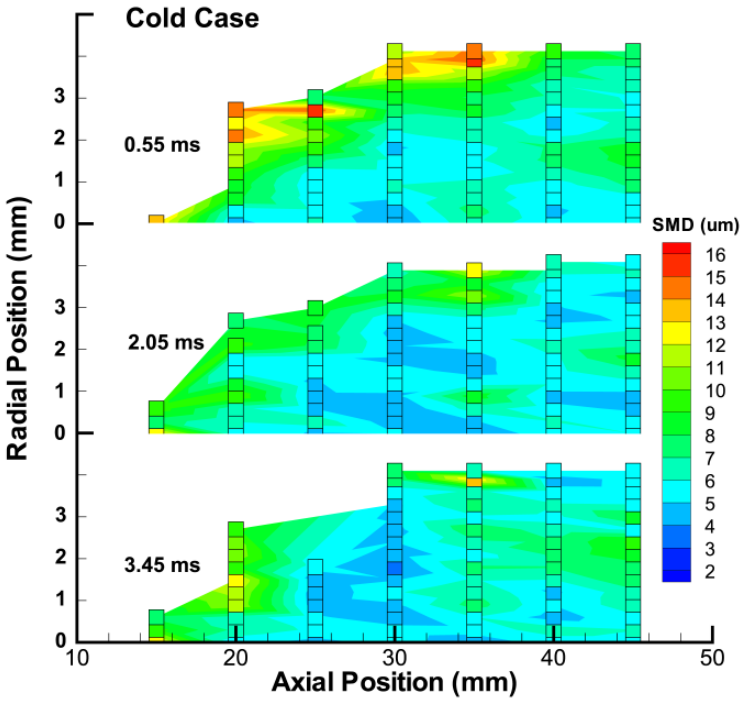

Fig. 12 Sauter mean diameter as a function of axial and radial position during each of the characteristic time periods [spray development (0.55 ms), steady state (2.05 ms), and spray dissipation (3.45 ms)] for the cold spray.

the data to be represented as contour plots of SMD and liquid volume fraction, as a function of the radial and axial coordinate, with one contour plot for each 100 μs in the spray development. Figures 9 and 10 are contour plots of the volume fraction (Figs. 11 and 12 show droplet sizes) as a function of axial and radial position for the times 0.55, 2.05, and 3.45 ms (which represent a 0.1 ms time average during spray development, steady state, and spray dissipation, respectively). Squares included in the plots are actual data point locations that have been shaded appropriately to reflect the value of the volume fraction at that point. Software is then used to interpolate between adjacent points to create the continuous plot. Full movies for all cases examined can be viewed online (see [11]).

The plots representing the 0.55 ms point in time show the spatial variation in the spray early on in the atomization process during the spray development period. The 2.05 ms plots illustrate the structure of the spray during the fully developed portion of the event (or steady state). The 3.45 ms data illustrate the volume fraction field at the time of spray shutoff. Note that Fig. 2 shows the transient injection pressure pulse along with relevant times.

DISCUSSION

For both combusting and room ambient cases, larger droplets exist at the spray periphery in comparison to the droplets at the spray centerline. As hypothesized previously [2], two possible mechanisms for this radial growth are collisional effects and vortex effects [12, 13]. Evaporation for the combusting case is expected to modify the spray compared to the cold case due to the elevated temperature. Compared to the combusting case, the cold case produced droplets at a radial distance further from the centerline, as well as a higher-density droplet region near the centerline. Competing effects contribute to this difference. The combusting (and evaporating) case was performed at an initial temperature of 873 K and 12.5 atm. pressure. The "cold" case was at 300 K and 0.8 atm. pressure (the ambient pressure in Denver, CO). The increased gas density for the combusting case produces a wider, more evenly distributed spray, explaining the lower centerline volume fraction for the combusting case. However, droplets at the spray periphery for the combusting case will readily evaporate. The cold case is essentially a nonevaporating spray (vapor pressure for dodecane at room temp is 2.7×10^{-5} atm.) Thus, the increase in gas density for the combusting case widens the spray, which produces a lower centerline volume fraction, but evaporation at the combusting spray edge limits the radial extent of the spray. From the perspective of where the volume fraction falls to undetectable levels (around 5×10^{-7}), the combusting spray is narrower. As an additional note, droplets of the sizes measured in this work would evaporate quickly unless the environment is saturated with fuel vapor. Therefore, detection of droplets on the order of a few microns indicates that the interior of the diesel spray is saturated or nearly saturated.

For both the cold and combusting spray, the volume fraction results depict a well-defined, thicker central region of the spray, indicating that a majority of the mixing/evaporation occurs at or near the spray periphery. Though the absolute values of volume fraction reported in Figs. 9 and 10 are different, an important common feature for the combusting and cold cases is that the volume fraction at the spray periphery is relatively steady for the times shown, including the postinjection period. In contrast, the central region for both sprays shows a significant decrease in volume fraction associated with the injection shutoff. This shows that the central, high mass bearing regions of the spray are tightly coupled to the mass exiting from the orifice and retain the majority of the momentum from the spray. The surrounding region, however, is a relatively low-velocity droplet bearing "cloud" of fuel droplets. This result has been noted in previous publications [1, 2] with the interpretation that the central core of the jet ejects mass to the edge where it relaxes to the local gas velocity in a very short time (and distance). One conclusion that can be drawn from data analysis is that the outer region of the spray is where a majority of the mixing and evaporating occurs and that this region has a relatively low-momentum level.

Comparing the cold data (Fig. 10) to the combusting data (Fig. 9), the liquid portion of the cold spray penetrates significantly further than that of the combusting spray (as shown by higher volume fractions at axial positions 40 and 45 mm from the tip). This is, once again, to be expected due to the increased background pressure and temperature, which act to enhance the mixing and evaporation at the spray periphery (including the penetrating spray tip). This trend of smaller penetration length with

increased pressure and temperature is not a new phenomenon; it has been reported by a host of other researchers [14–16].

A theoretical correlation put forth by Higgins et al. [17] applied to the combusting case conditions in this article predicts the penetration length of the combusting spray to be 32 mm. Experimentally, the average liquid penetration length during steady state (defined as the axial position at which liquid volume fraction levels fall to < 10% of maximum levels) was estimated to be 31.6 mm for the combusting case. The correlation was not applicable to the cold case, and experimentally, the liquid penetration length was > 45 mm, which was outside of the measurement region.

Experimentally, the full angle at which the cold spray spread was ~ 7°, the combusting spray spread at 10° (again, based on 10% of centerline volume fraction levels). Note that previously developed correlations [18] would indicate a full spread angle of ~ 4° for the cold case and 7° for the combusting case. However, this correlation includes an empirical constant for the hole type and this constant was difficult to accurately determine for the injector used in this work. In addition, the 4° and 7° values are based on a nonquantitative measure of the spray.

Finally, it is interesting to note that the cold spray has three distinct and repeatable high-volume fraction "zones" throughout the steady-state time period (see Fig. 10). These zones are ~ 20–25 mm from the tip and approximately on axis, near 30 mm from the tip axially and ~ 2.5 mm from the centerline, and near 40 mm from the tip and ~ 4 mm from the centerline. Observation of these zones is the most apparent when viewing the data in "movie" format [11]. These zones have an appearance and behavior similar to vortices or recirculation zones, but the authors have no evidence, other than the scattering data presented in this article, that these high-concentration zones are vortices. However, the observation of this type of structure within the spray illustrates that interior fluid mechanics may be more structured than that predicted by a simple entraining jet. Specifically, the possibility of behavior similar to that for a shear layer between the high-momentum interior jet and the low-velocity, liquid-bearing cloud that surrounds the cloud is intriguing.

CONCLUSIONS

- The results presented here are the first of their kind in that spray properties from cold and combusting diesel sprays were presented as a function of axial and radial position. Globally, the cold spray formed larger droplets and resulted in a region of higher liquid volume fraction levels compared to the combusting spray. For both cases, the largest droplets formed by each spray were reported at the spray periphery.
- Both cases showed that the spray is transient in nature. Three distinct time periods are discernable: spray development period (0–0.75 ms), steady-state period (0.75–3.0 ms), and spray dissipation period (> 3.0 ms). For both cases, every position examined exhibited these temporal dependencies.
- The volume fraction data indicate that evaporation is significantly more prevalent in the combusting spray than the cold spray. Examining the cold data, it is concluded that more of the fuel mass is in the liquid form compared to the combusting case. This is expected due to the increased temperature and pressure of the background air. Additionally, results from both cases indicate that the central region of the jet is fuel-vapor saturated. For the time scales presented, droplets of such small sizes (5 μm and below) can only exist if the surrounding gas is saturated, making further evaporation of the droplet impossible without additional mixing with air.
- The liquid penetration lengths for each case also indicate that significantly more of the fuel mass is vaporized for the combusting case than for the cold case. The liquid penetration length for the combusting case was near the expected theoretical value of 32 mm, whereas the penetration length for the cold case was > 45 mm. From this result, it can be concluded that the increased background temperature and pressure enhance the mixing and vaporization process.
- The trend in SMD over the spray, for both combusting and room ambient cases, was an increase in size with an increase in radial and axial distance. Thus, for the spray locations investigated, the smallest droplets were on axis and close to the injector tip.

- An interior structure in the spray similar to what one would expect for vortices was observed. In addition, the spray interior for both cases, consistent with previous observations [2], exhibited behavior consistent with high momentum compared to the spray periphery.

REFERENCES

1. T. E. Parker, L. R. Rainaldi, and W. T. Rawlins, A Comparative Study of Room Temperature and Combusting Fuel Sprays Near the Injector Tip Using Infrared Laser Diagnostics, *Atomization and Sprays*, vol. 8, pp. 565–600, 1998.
2. J. E. Labs and T. E. Parker, Diesel Fuel Spray Droplet Sizes and Volume Fractions from the Region 25 mm Below the Orifice, *Atomization and Sprays*, vol. 13, nos. 5–6, pp. 425–442, 2003.
3. J. B. Heywood, *Internal Combustion Engine Fundamentals*, McGraw-Hill, New York, pp. 586–587, 1988.
4. Y. Yue, C. F. Powell, R. Poola, J. Wang, and J. K. Schaller, Quantitative Measurements of Diesel Fuel Spray Characteristics in the Near-Nozzle Region Using X-Ray Absorption, *Atomization and Sprays*, vol. 11, pp. 471–490, 2001.
5. A. G. MacPhee, M. W. Tate, C. F. Powell, Y. Yue, J. Renzi, A. Ercan, S. Narayanan, E. Fontes, J. Walther, J. Schaller, S. M. Gruner, and J. Wang, X-ray Imaging of Shock Waves Generated by High-Pressure Fuel Sprays, *Science*, vol. 295, pp. 1261–1263, 2002.
6. T. E. Parker, E. Jepsen, and H. McCann, Measurements and Error Analysis of Droplet Size in Optically Thick Diesel Sprays, in *Twenty-Seventh International Symposium on Combustion*, The Combustion Institute, pp. 1881–1888, 1998.
7. D. Oren, R. P. Durret, C. R. Fergusen, J. Timar, D. R. Tree, and D. P. DeWitt, A Multidimensional Data Set for Diesel Combustion Model Validation: II - Fuel Injection Rate and Boundary Conditions, SAE Paper No. 872088, 1987.
8. J. E. Labs, J. Filley, E. Jepsen, and T. E. Parker, A Detailed Review of a Constant Volume Diesel Spray Combustion Facility and the Corresponding Experimental Diagnostics, *Rev. Sci. Instr.*, vol. 76, no. 3, 11 pp., 2005.
9. K. Kohse-Hoinghaus, Laser Techniques for the Quantitative Detection of Reactive Intermediates in Combustion Systems, *Prog. Energy Combust. Sci.*, vol. 20, pp. 203–279, 1994.
10. J. Labs and T. E. Parker, Multiple Scattering Effects on Infrared Scattering Measurements Used to Characterize Droplet Size and Volume Fraction Distributions in Diesel Sprays, *Appl. Opt.*, vol. 44, no. 28, pp. 6049–6057, 2005.
11. http://www.begellhouse.com/video/6a7c7e10642258cc/smd_movie_cold.avi
    http://www.begellhouse.com/video/6a7c7e10642258cc/smd_movie_comb.avi
    http://www.begellhouse.com/video/6a7c7e10642258cc/vf_movie_cold.avi
    http://www.begellhouse.com/video/6a7c7e10642258cc/vf_movie_comb.avi
12. K. J. Wu, R. D. Reitz, and F. V. Bracco, Measurements of Drop Size at the Spray Edge near the Nozzle in Atomizing Liquid Jets, *Phys. Fluids*, vol. 29, no.4, pp. 941–951, 1986.
13. C. Yeh, H. Kosaka, and T. Kamimoto, Measurement of Drop Sizes in Unsteady Dense Sprays, in *Recent Advances in Spray Combustion: Spray Atomization and Drop Burning Phenomena*, American Institute of Aeronautics and Astronautics, Reston, VA, pp. 297–308, 1995.
14. C. Espey and J. E. Dec, The Effect of TDC Temperature and Density on the Liquid-Phase Fuel Penetration in a DI Diesel Engine, SAE Paper No. 952456, 1995.
15. D. Siebers, Scaling Liquid-Phase Fuel Penetration in Diesel Sprays Based on Mixing-Limited Vaporization, SAE Paper No. 1999-01-0528. 1999.
16. V. A. Iyer, S. L. Post, and J. Abraham, Is the Liquid Penetration in Diesel Sprays Mixing Controlled? in *Proc. of the Combustion Institute*, Combustion Inst. Pittsburgh, vol. 28, pp. 1111–1118, 2000.
17. B. S. Higgins, C. J. Mueller, and D. L. Siebers, Measurements of Fuel Effects on Liquid-Phase Penetration in DI Sprays, SAE Paper No. 1999-01-0519. 1999.
18. K.-J. Wu, C.-C. Su, R. L. Steinberger, D. A. Santavicca, and F. V. Bracco, Measurements of the Spray Angle of Atomizing Jets, *ASME J. Fluids Eng.*, vol. 105, pp. 406–413, 1983.